Applied Physics Letters

RESEARCH ARTICLE | FEBRUARY 28 2024

Molecular beam epitaxy growth of superconducting tantalum germanide

Patrick J. Strohbeen ; Tathagata Banerjee ; Aurelia M. Brook ; Ido Levy ; Wendy L. Sarney ; Jechiel van Dijk; Hayden Orth ; Melissa Mikalsen ; Valla Fatemi ; Javad Shabani

Appl. Phys. Lett. 124, 092102 (2024)
https://doi.org/10.1063/5.0189597

Applied Physics Letters ARTICLE pubs.aip.org/aip/apl

Molecular beam epitaxy growth of superconducting tantalum germanide

Cite as: Appl. Phys. Lett. **124**, 092102 (2024); doi: 10.1063/5.0189597
Submitted: 30 November 2023 · Accepted: 5 February 2024 ·
Published Online: 28 February 2024

Patrick J. Strohbeen,[1] Tathagata Banerjee,[2] Aurelia M. Brook,[1] Ido Levy,[1] Wendy L. Sarney,[3] Jechiel van Dijk,[1] Hayden Orth,[1] Melissa Mikalsen,[1] Valla Fatemi,[2] and Javad Shabani[1,a)]

AFFILIATIONS

[1]Center for Quantum Information Physics, Department of Physics, New York University, New York, New York 10003, USA
[2]School of Applied and Engineering Physics, Cornell University, Ithaca, New York 14853, USA
[3]Army Research Directorate, DEVCOM Army Research Laboratory, Adelphi, Maryland 20783, USA

[a)]**Author to whom correspondence should be addressed:** jshabani@nyu.edu

ABSTRACT

Developing alternative material platforms for use in superconductor–semiconductor hybrid structures is desirable due to limitations caused by intrinsic microwave losses present in commonly used III/V material systems. With the recent reports on tantalum superconducting qubits that show improvements over the Nb and Al counterparts, exploring Ta the superconductor in hybrid material systems is promising. Here, we study the growth of Ta on semiconducting Ge (001) substrates grown via molecular beam epitaxy. We show that at a growth temperature of 400 °C, the Ta diffuses into the Ge matrix in a self-limiting nature resulting in smooth and abrupt surfaces and interfaces with roughness on the order of 3–7 Å as measured by atomic force microscopy and x-ray reflectivity. The films are found to be a mixture of Ta_5Ge_3 and $TaGe_2$ binary alloys and form a native oxide that seems to form a sharp interface with the underlying film. These films are superconducting with a $T_C \sim 1.8 - 2$ K and $H_C^{\perp} \sim 1.88$ T, $H_C^{\parallel} \sim 5.1$ T. These results show this tantalum germanide film to be promising for future superconducting quantum information platforms.

Superconductor–semiconductor (S–Sm) hybrid material platforms have been of interest in the last few decades for studying mesoscopic superconductor physics,[1] the search for topological superconductivity,[2,3] and most recently for the development of new voltage-tunable qubits, couplers, and other superconducting circuit elements.[4–6] However, due to the complexity of the material requirements (e.g., interface roughness and band alignment), growth of these structures is not straightforward. Furthermore, in terms of the latter application in superconducting circuitry for circuit quantum electrodynamics (cQED), high intrinsic losses in the community standard Al–InAs system[4] have motivated material exploration studies to search for materials better suited toward these cQED applications. On the other hand, recent advancements in the Si–Ge alloy system present these materials to be highly promising for low-microwave loss materials[7–16] for quantum information applications.

In terms of superconducting materials, implementation of tantalum metal is also extremely interesting for cQED devices due to the fact that it forms a well-behaved native oxide for superconducting microwave applications.[17–19] Additionally, recent studies showed that this behavior of Ta also propagates to high-performance cQED devices.[20,21] In this context, major increases in qubit coherence times are caused by low intrinsic two-level system (TLS) losses within the Ta metal native oxide, Ta_2O_5.[20,21] However, implementation of this material into S–Sm hybrid materials requires significant effort in terms of understanding the film growth parameters to promote smooth interfaces/surfaces. Thus, further study of Ta and Ta-alloys is of interest for alternative S-Sm hybrid material systems.

Here, we report the diffusion-limited growth (diffusion-growth) of tantalum germanide films via molecular beam epitaxy (MBE). This technique is similar to what has been previously employed to study superconducting contacts in GaAs/AlGaAs systems.[22] We evaluate our grown films via a suite of structural and electronic material characterization and present the chemical composition, structure, and superconductivity behavior of this material. We demonstrate a unique growth method that forms uniform, wafer-scale thin films of homogeneous chemical composition and thickness that make this material system highly promising for future applications in superconducting cQED devices.

The tantalum germanide films are grown on 50.8 mm Ge(001) substrates in a custom solid-source molecular beam epitaxy system

(Mod Gen II) equipped with three electron beam sources and hydrogen cleaning capabilities. The internal manifold around the sources is water-cooled and no LN_2 cryo-paneling is used during this deposition. The substrates are first etched *ex situ* in de-ionized water at 90 °C for 15 min and then immediately loaded into vacuum on indium-free blocks. The substrates are initially outgassed in the growth reactor at 200 °C for 15 min before slowly increasing the temperature to 550 °C to anneal them for 10 min. We confirm the removal of the surface oxide via *in situ* reflection high-energy electron diffraction (RHEED) monitoring. We use the presence of a well-defined and sharp (2 × 1) surface reconstruction of the Ge (001) facet to indicate the removal of any native oxide that re-forms during the substrate mounting process. Ta deposition was done using a water-cooled vertical EBVV e-beam source from MBE Komponenten at an emission current of 180 mA in a 6 kV acceleration field. The films are grown at 400 °C, immediately following the Ge oxide removal. Due to passive heating from the Ta source, deposition was conducted in three cycles of 10 min each, allowing the chamber to cool for 15 min between deposition cycles to prevent significant outgassing from the chamber walls.

Figure 1 presents x-ray diffraction data taken using a Bruker D8 Discovery lab source diffractometer with a da Vinci configuration and a conditioned Cu Kα_1 source. A collimator and 1 mm slit are used to reduce the effects of substrate bowing in select measurements. All scans are measured in a double crystal configuration. An out-of-plane $\theta - 2\theta$ scan is presented in Fig. 1(a) in which the only reflection visible is the substrate Ge (004) reflection at 66°. X-ray reflectivity (XRR) measurements are taken after removing the collimator and reducing the slits to 0.2 mm. The XRR results are presented in Fig. 1(b), showing extremely sharp interfaces for the amorphous film. The fit is initialized assuming a two-layer model for the film structure with the primary layer being a film of tantalum germanide of composition $TaGe_2$, and the secondary layer being a thin native oxide layer of composition $Ta_2Ge_2O_9$. Since the density is unknown due to the amorphous nature, we allow the scattering length density (SLD) to vary in the fitting procedure. The results of the fit are shown in Table I. The feature that is not captured by our fitting model, we speculate, is related to the dot-like features observed in the atomic force microscopy (AFM) image seen in Fig. 1(c). These features are well dispersed across the sample surface and are all nominally of uniform thickness and may be the cause of this spurious peak that is not captured by our two-layer model. The roughness values for the fits are initialized at 7 Å, the roughness we measured in AFM, but are allowed to vary for both layers individually.

TABLE I. X-ray reflectivity fitting results.

Layer	SLD (10^{-6}/Å^2)	Thickness (Å)	Roughness (Å)
Tantalum germanide	93.97	175.1	3.6
Native oxide	64.95	24.4	9.3

From the fits, we extract SLD values for total internal reflection x-ray scattering in the XRR measurements. Using the following equation, we then calculate the product of $\rho f_1/M_a$, relating the SLD from the fit back to the material density and scattering factor,

$$\mathrm{Re}(SLD) = \frac{\rho N_a r_e}{M_a} f_1, \tag{1}$$

where ρ is the material density, N_a is Avogadro's constant, r_e is the classical electron radius ~2.818 × 10^{-15} m, M_a is the molar mass, and f_1 is the real part of the atomic scattering factor of the compound. We calculate values of 5.54 and 3.83 cm^{-3} for the tantalum germanide and native oxide layers, respectively.

Crystallinity and interface structure of the tantalum germanide film is examined with scanning transmission electron microscopy (STEM) in a JEOL ARM200F, equipped with a spherical aberration corrector for the probe mode, and operated at 200 keV. The samples were prepared with cross-sectional tripod polishing to 20 μm thickness, followed by shallow angle Ar+ ion milling with low beam energies ([1]3 keV) and LN2 stage cooling in a PIPS II ion mill. Exemplary transmission electron microscopy images are shown in Fig. 2, where we observe sharp interfaces and well-defined film and oxide regions of thicknesses ~18.7 and ~2.2 nm for the film and oxide, respectively, which are in good agreement with the XRR measurements. Energy dispersive x-ray spectroscopy (EDS) was conducted in an Oxford Aztec system and is presented in Fig. S1 in the supplementary material.

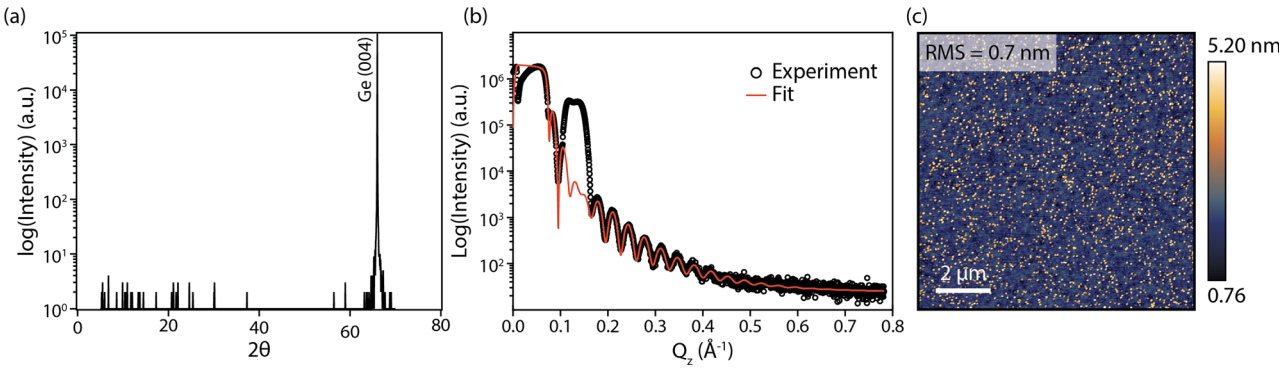

FIG. 1. X-ray diffraction characterization of a tantalum germanide film. (a) Out-of-plane θ–2θ scan. The only distinct reflection is from the Ge substrate. (b) X-ray reflectivity measurement of the tantalum germanide film. The fit is done using REFLEX[23] standalone reflectivity fitting software, assuming two layers of composition, $TaGe_2$ and $Ta_2Ge_2O_9$, as initial conditions. (c) 10 × 10 μm^2 AFM image of tantalum germanide surface. RMS value of 7 Å was used as the initial roughness for the XRR fitting.

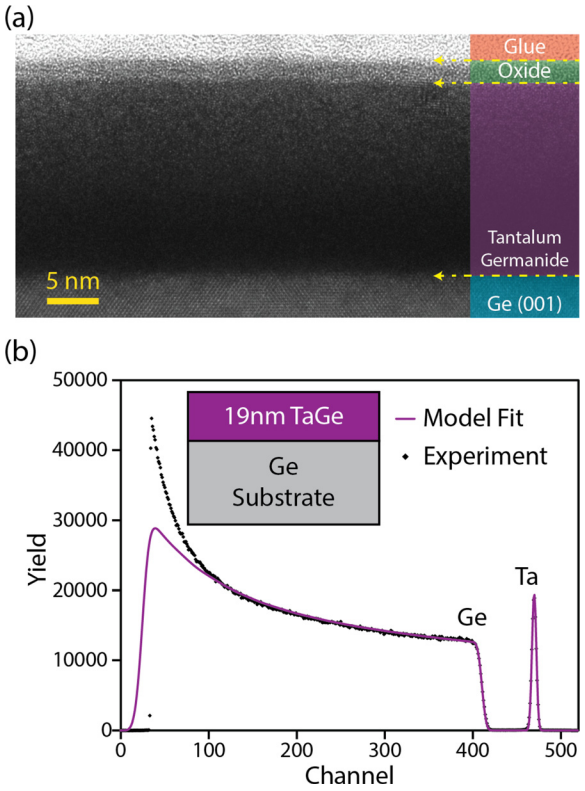

FIG. 2. TEM imaging of tantalum germanide film. (a) Zoomed-out image of tantalum germanide lamella that shows sharp interfaces at the oxide-film and film-substrate interfaces. (b) RBS trace for the tantalum germanide film. The black dots and trace are the experimental data and the purple line is the model fit. The inset presents the model used to generate the fit.

From compositional mapping, a thickness of ∼18.2 nm for the film is found, which is in good agreement with our TEM imaging.

For an accurate determination of the full film composition, Rutherford backscattering spectroscopy measurements were conducted via EAG Eurofins using a Cornell measurement geometry. The He^{++} ion beam energy was set to 2.275 MeV He^{++}, and the detector was placed at an angle of 160° from the ion beam path. A second grazing incidence detector was placed at 100° to increase measurement accuracy. Figure 2(b) presents the RBS data collected at the detector 160° from the beam path. From these measurements, we calculate the film stoichiometry to be $\sim 58.5 \pm 0.5 : 41.5 \pm 1$ Ta:Ge ratio, or a chemical formula of roughly Ta_3Ge_2. Using the Ta–Ge binary phase diagram,[24] the film is likely a solid solution of 86.3% Ta_5Ge_3 and 13.7% $TaGe_2$. Exact composition of the oxide layer is unable to be determined via RBS. Depth-resolved x-ray photoemission spectroscopy (XPS) shows a nominally constant composition throughout the film layer, as seen in the supplementary material in Fig. S2, similar to what is observed in the EDS measurement. The composition of the film as measured in XPS is more consistent with the RBS measurement, and the oxide region is similar to what is observed in EDS. We note that the three different methods of RBS, XPS, and EDS report varying Ta concentrations where XPS reports the film to be Ta-rich, EDS reports a stark Ta deficiency, and RBS reports a Ta_5Ge_3-rich mixture of Ta_5Ge_3 and $TaGe_2$ phases. For the remainder of this work, we take the RBS measurement to be the true absolute measure of film composition.

For determining the density of the film, we use the value of composition as reported from our RBS measurements. Assuming random distribution of elemental species in the two distinct layers, we then calculate the expected average material density to be 14.39 g/cm^3 for the tantalum germanide layers, respectively. Comparing against the density of the crystalline form, approximated to be 13.82 g/cm^3[25,26] for the binary solution, this amorphous film exhibits a ∼4% increase in density. This increase in density is attributed to the amorphous nature of the film, which has been seen previously for pure germanium.[27]

Magnetotransport measurements of this material are done in an Oxford Triton dry dilution refrigerator with a base temperature of 15 mK and a single direction magnet with a maximum field of 14 T. Samples are cleaved down to roughly 5×5 mm^2 chips. Contacts on the chip are made by annealing In–Sn eutectic into the four corners in a Van der Pauw geometry, which are then contacted to the sample board via gold wires. The results of these measurements are presented in Fig. 3. We see a sharp transition to a zero resistance state at roughly 2 K upon cooldown, as shown in Fig. 3(a). To investigate the field dependance, we sweep out-of-plane and in-plane magnetic field as

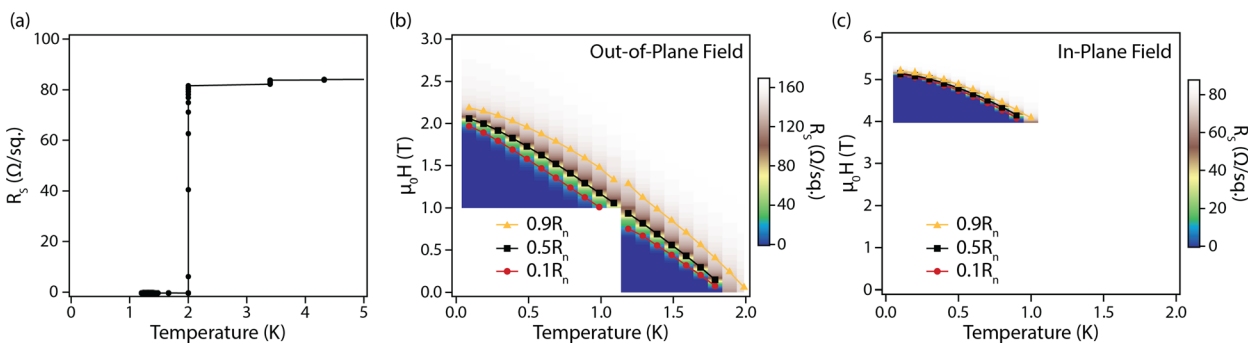

FIG. 3. Magnetotransport data of the tantalum germanide film. (a) Cooldown trace of sheet resistance, R_S. We see a zero-resistance transition near 2 K. (b) R_S map as a function of applied out-of-plane field and temperature. Lines are fits to the 0.9, 0.5, and 0.1R_n values. (c) R_S map for in-plane magnetic field configuration.

shown in Figs. 3(b) and 3(c), respectively. The resistance surface presented in Fig. 3(b) shows a very sharp transition from the superconducting phase to the normal state, suggestive of type 1 superconductivity. This is observed in the tight spread of $0.9R_n$, $0.5R_n$, and $0.1R_n$ contours overlaid on the color map. For out-of-plane field configuration, we observe a critical applied field of $H_C \sim 1.88$ T. The critical field fitting gives us a critical temperature of roughly 1.8 K. This temperature is similar to the reported range of T_C of 2.3–2.75 K for compositions of $x = 17\%$–55% in the Ta_xGe_{1-x} alloy system,[28] which also agrees well with our RBS composition data. With an in-plane field configuration, we measure a critical applied field of $H_C \sim 5.1$ T that also exhibits a sharp superconducting transition up to 1 K. We present these data in Fig. 3(c) in which we overlay the $0.9R_n$, $0.5R_n$, and $0.1R_n$ contours. The variation in sheet resistance between Fig. 3(b) and Figs. 3(a) and 3(c) are a result of oxidation in the film over the course of roughly 6 months causing an increase in film resistance. The measurements were otherwise conducted on the exact same sample.

In conclusion, we presented here the growth, structure, and transport characteristics of diffusion-grown tantalum germanide thin films grown via MBE. The tantalum germanide films are formed by a semi-rate-limited diffusion process in which the e-beam evaporated Ta diffuses into the surface that preserves a 3 : 2 Ta:Ge composition ratio within the film region. These films form a small native oxide layer with sharp interfaces and exhibit a roughly 4% increase in material density. Transport shows a reasonable critical temperature of ~1.8–2 K, but we increasingly find a critical out-of-plane and in-plane critical field of $H_C^{\perp} \sim 1.88$ T and $H_C^{\parallel} \sim 5.1$ T, respectively. With such a high critical field, ease of semiconductor integration, and the preservation of sharp S–Sm interfaces, this material shows promise for integration into cQED devices.

See the supplementary material for additional details on the EDS and XPS experimental considerations and analysis. The data presented herein shows the depth-resolved elemental profiles for the tantalum germanide film as an image via EDS as well as XPS core-level measurements as a function of sputtering depth.

The authors would like to acknowledge funding support for this project by AFOSR Award No. FA9550-21-1-0338. The authors gratefully acknowledge the use of facilities and instrumentation supported by the NSF through the Cornell University Materials Research Science and Engineering Center (DMR-1719875).

AUTHOR DECLARATIONS

Conflict of Interest

The authors have no conflicts to disclose.

Author Contributions

Patrick James Strohbeen: Conceptualization (lead). **Tathagata Banerjee:** Investigation (equal); Validation (equal). **Aurelia Meiqi Brook:** Investigation (supporting). **Ido Levy:** Investigation (supporting). **Wendy L. Sarney:** Visualization (supporting). **Jechiel van Dijk:** Investigation (supporting). **Hayden Orth:** Investigation (supporting). **Melissa Mikalsen:** Investigation (supporting). **Valla Fatemi:** Investigation (equal); Methodology (equal); Validation (equal); Writing – review & editing (equal). **Javad Shabani:** Supervision (lead).

DATA AVAILABILITY

The data that support the findings of this study are available from the corresponding author upon reasonable request.

REFERENCES

[1]F. Rahman, T. J. Thornton, R. Huber, L. F. Cohen, W. T. Yuen, and R. A. Stradling, "Superconductor-semiconductor interaction effects in mesoscopic hybrid structures," Phys. Rev. B **54**, 14026–14031 (1996).
[2]V. Mourik, K. Zuo, S. M. Frolov, S. R. Plissard, E. P. A. M. Bakkers, and L. P. Kouwenhoven, "Signatures of Majorana fermions in hybrid superconductor-semiconductor nanowire devices," Science **336**, 1003–1007 (2012).
[3]E. Prada, P. San-Jose, M. W. A. de Moor, A. Geresdi, E. J. H. Lee, J. Klinovaja, D. Loss, J. Nygård, R. Aguado, and L. P. Kouwenhoven, "From Andreev to Majorana bound state in hybrid superconductor-semiconductor nanowires," Nat. Rev. Phys. **2**, 575–594 (2020).
[4]L. Casparis, M. R. Connolly, M. Kjaergaard, N. J. Pearson, A. Kringhøj, T. W. Larsen, F. Kuemmeth, T. Wang, C. Thomas, S. Gronin, G. C. Gardner, M. J. Manfra, C. M. Marcus, and K. D. Petersson, "Superconducting gatemon qubit based on a proximitized two-dimensional electron gas," Nat. Nanotechnol. **13**, 915–919 (2018).
[5]G. Burkard, M. J. Gullans, X. Mi, and J. R. Petta, "Superconductor-semiconductor hybrid-circuit quantum electrodynamics," Nat. Rev. Phys. **2**, 129–140 (2020).
[6]W. M. Strickland, B. H. Elfeky, J. O. Yuan, W. F. Schiela, P. Yu, D. Langone, M. G. Vavilov, V. E. Manucharyan, and J. Shabani, "Superconducting resonators with voltage-controlled frequency and nonlinearity," Phys. Rev. Appl. **19**, 034021 (2022).
[7]M. Sandberg, V. P. Adiga, M. Brink, C. Kurter, C. Murray, M. Hopstaken, J. Bruley, J. S. Orcutt, and H. Paik, "Investigating microwave loss of SiGe using superconducting transmon qubits," Appl. Phys. Lett. **118**, 124001 (2021).
[8]G. Scappucci, C. Kloeffel, F. A. Zwanenburg, D. Loss, M. Myronov, J.-J. Zhang, S. D. De Franceschi, G. Katsaros, and M. Veldhorst, "The germanium quantum information route," Nat. Rev. Mater. **6**, 926–943 (2020).
[9]M. Lodari, O. Kong, M. Rendell, A. Tosato, A. Sammak, M. Veldhorst, A. R. Hamilton, and G. Scappucci, "Lightly strained germanium quantum wells with hole mobility exceeding one million," Appl. Phys. Lett. **120**, 122104 (2022).
[10]A. Sarkar, Z. Wang, M. Rendell, N. W. Hendrickx, M. Veldhorst, G. Scappucci, M. Khalifa, J. Salfi, A. Saraiva, A. S. Dzurak, A. R. Hamilton, and D. Culcer, "Electrical operation of planar Ge hole spin qubits in an in-plane magnetic field," Phys. Rev. B **108**, 245301 (2023).
[11]M. Myronov, J. Kycia, P. Waldron, W. Jiang, P. Barrios, A. Bogan, P. Coleridge, and S. Studenikin, "Holes outperform electrons in group IV semiconductor materials," Small Sci. **3**, 2200094 (2023).
[12]J. M. Hartmann, N. Bernier, F. Pierre, J. P. Barnes, V. Mazzocchi, J. Krawczyk, G. Lima, E. Kiyooka, and S. De Franceschi, "Epitaxy of group-IV semiconductors for quantum electronics," ECS Trans. **111**, 53 (2023).
[13]M. Myronov, P. Waldron, P. Barrios, A. Bogan, and S. Studenikin, "Electric field-tuneable crossing of hole Zeeman splitting and orbital gaps in compressively strained germanium semiconductor on silicon," Commun. Mater. **4**, 104 (2023).
[14]Y.-X. Li, Z. Kong, S. Hou, G. Wang, and S. Huang, "Quantum transport quality of a processed undoped Ge/SiGe heterostructure," Phys. Rev. B **108**, 045303 (2023).
[15]A. Tosato, V. Levajac, J.-Y. Wang, C. J. Boor, F. Borsoi, M. Botifoll, C. N. Borja, S. Martí-Sánchez, J. Arbiol, A. Sammak, M. Veldhorst, and G. Scappucci, "Hard superconducting gap in germanium," Commun. Mater. **4**, 23 (2023).
[16]Z. Kong, Z. Li, G. Cao, J. Su, Y. Zhang, J. Liu, J. Liu, Y. Ren, H. Li, L. Wei, G-p Guo, Y. Wu, H. H. Radamson, J. Li, Z. Wu, H-o Li, J. Yang, C. Zhao, T. Ye, and G. Wang, "Undoped strained Ge quantum well with ultrahigh mobility of two million," ACS Appl. Mater. Interfaces **15**, 28799–28805 (2023).
[17]L. Y. L. Shen, *Superconductivity in d- and f-Band Metals*, edited by D. H. Douglass (Springer, 1972).
[18]E. G. Spencer and J. M. Rowell, "Superconductivity of Ta-Zr films produced by co-sputtering," IEEE Trans. Magn. **17**, 322–325 (1981).

[19]D. W. Face, D. E. Prober, W. R. McGrath, and P. Richard, "High quality tantalum superconducting tunnel junctions for microwave mixing in the quantum limit," Appl. Phys. Lett. **48**, 1098–1100 (1986).
[20]A. P. M. Place, L. V. H. Rodgers, P. Mundada, B. M. Smitham, M. Fitzpatrick, Z. Leng, A. Premkumar, J. Bryon, A. Vrajitoarea, S. Sussman, G. Cheng, T. Madhavan, H. K. Babla, X. H. Le, Y. Gang, B. Jäck, A. Gyenis, N. Yao, R. J. Cava, N. P. de Leon, and A. A. Houck, "New material platform for superconducting transmon qubits with coherence times exceeding 0.3 milliseconds," Nat. Commun. **12**, 1779 (2021).
[21]R. A. McLellan, A. Dutta, C. Zhou, Y. Jia, C. Weiland, X. Gui, A. P. M. Place, K. D. Crowley, X. H. Le, T. Madhavan, Y. Gang, L. Baker, A. R. Head, I. Waluyo, R. Li, K. Kisslinger, A. Hunt, I. Jarrige, S. A. Lyon, A. M. Barbour, R. J. Cava, A. A. Houck, S. L. Hulbert, M. Liu, A. L. Walter, and N. P. de Leon, "Chemical profiles of the oxides on tantalum in state of the art superconducting circuits," Adv. Sci. **10**, 2300921 (2023).
[22]J. R. Gao, J. J. B. Kerkhof, M. Verwerft, P. Magnée, B. J. van Wees, T. M. Klapwijk, and J. T. M. De Hosson, "Analysis of superconducting Sn/Ti contacts to GaAs/AlGaAs heterostructures by electron focusing," Semicond. Sci. Technol. **11**, L621–624 (1996).
[23]G. Vignaud and A. Gibaud, "REFLEX: A program for the analysis of specular X-ray and neutron reflectivity data," J. Appl. Crystallogr. **52**, 201–213 (2019).
[24]A. A. A. Pinto da Silva, G. C. Coelho, C. A. Nunes, P. A. Suzuki, J. M. Fiorani, N. David, and M. Vilasi, "Experimental determination of the Ta-Ge phase diagram," J. Alloys Compd. **576**, 38–42 (2013).
[25]L. H. Brixner, "X-ray study and thermoelectric properties of the $NbSi_xGe_{2-x}$ and the $TaSi_xGe_{2-x}$ systems," J. Inorg. Nucl. Chem. **25**, 257–260 (1963).
[26]F. Yuan, S. Forbes, K. K. Ramachandran, and Y. Mozharivskyj, "Structure and physical properties of Cr_5B_3-type Ta_5Si_3 and Ta_5Ge_3," J. Alloys Compd. **650**, 712–717 (2015).
[27]J. R. Blanco, P. J. McMarr, J. E. Yehoda, K. Vedam, and R. Messier, "Density of amorphous germanium films by spectroscopic ellipsometry," J. Vac. Sci. Technol. A **4**, 577–582 (1986).
[28]A. K. Ghosh and D. H. Douglass, "Superconductivity in transition metal-germanium systems," J. Low Temp. Phys. **27**, 487–512 (1977).